International Journal of Pressure Vessels and Piping 207 (2024) 105100

Contents lists available at ScienceDirect

International Journal of Pressure Vessels and Piping

journal homepage: www.elsevier.com/locate/ijpvp

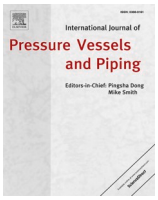

Time-dependent reliability of corroded mild steel pipes by different failure modes

Bohua Zhang [a], Haoran Lei [a], Xiancun Hu [b], Chun-Qing Li [a,*]

[a] School of Engineering, RMIT University, Melbourne, 3001, Australia
[b] School of Design and the Built Environment, University of Canberra, Canberra, ACT, 2617, Australia

ARTICLE INFO

Keywords:
Time-dependent reliability
Fracture failure
Mild steel pipes
Pitting corrosion
Elastic-plastic fracture mechanics

ABSTRACT

This study aims to analytically assess the time-dependent failure of corrosion-induced mild steel pipes by employing two fracture failure criteria: the fracture toughness-based criterion and the stress-based criterion. The investigation intends to identify the influential factors that impinge upon the assessment of failure probability within this context. It is found that there is a linear relationship between the ratio of wall thickness to inner radius and the probability of failure and that between the internal pressure and the probability of failure. Notably, the influence on the evaluation of failure probability by the ratio of wall thickness to inner radius is more prominent than the internal pressure. It is also found that a comprehensive criterion is necessary for evaluating the fracture resistance of corroded mild steel pipes, which considers both initial fracture toughness and ultimate stress. These findings can provide theoretical evidence for pipe engineers to develop maintenance or repair strategies in mild steel pipes. The significance of this paper is the development of an analytical framework for predicting the probability of failure of corroded mild steel pipes, considering the complexities of elastic-plastic fracture mechanics.

1. Introduction

Pipes play a pivotal role in various sectors, serving as critical infrastructure for transporting fluids, for example, oil, gas, water and chemicals, over long distances, and facilitating economic growth, resource utilisation and societal wellbeing. It is important to note that pipelines also present challenges and risks, such as potential leaks or spills. Proper maintenance and repair are essential to ensure the integrity and safety of pipelines, as well as to protect the environment and communities along their routes. Time-dependent assessments of pipe reliability can provide guidance for establishing maintenance and repair strategies. Therefore, it is of practical significance to thoroughly investigate failure mechanisms, establish suitable stochastic models and develop effective time-dependent methods to predict the failure of pipelines.

Narrow and sharp corrosion damage is considered more critical than blunt damage because it acts as an initial crack and facilitates subsequent fractures in pipes. Pitting corrosion is a prevalent mode of failure observed in metallic pipes, for example, cast iron, ductile iron and steel. Research findings indicated that cast-iron pipes exhibit the highest potential for failure attributed to corrosion, followed by steel pipes [1]. The occurrence of corrosion pits in pipes weakens their structural integrity and, thus, leads to fluids loss [2]. Research conducted by Ref. [3] revealed that corrosion pitting constituted 51 % of all water pipe failures in a network, while fitting failure and mechanical damage accounted for 26 % and 6 % of failures, respectively.

Unlike brittle pipes, the fracture behaviour of steel pipes is a progressive process with a steady crack growth during which plastic deformation occurs around the defect or damage. It is necessary to assess the failure probability of steel pipes using elastic-plastic fracture mechanics (EPFM)-based methods. Additionally, the fracture resistance of steel pipes depends on the extent of crack propagation and the size of defects or damages. Thus, the employed failure criterion must be periodically updated at different time points throughout the whole process of evaluating pipe reliability. Therefore, accurate predictions of fracture failure of corroded steel pipes necessitate stochastic models developed based on actual inspection databases. Moreover, the identification of factors exerting influence on pipe deterioration becomes an essential component for the formulation of such stochastic models [4]. By identifying these significant factors, the number of variables required and the associated data collection costs can be reduced, leading to a more accurate stochastic model [5].

* Corresponding author.
E-mail address: chunqing.li@rmit.edu.au (C.-Q. Li).

https://doi.org/10.1016/j.ijpvp.2023.105100
Received 18 October 2023; Received in revised form 13 November 2023; Accepted 20 November 2023
Available online 25 November 2023

Numerous models have been proposed to assess the failure probability of corroded brittle pipes, such as those by Refs. [6,7]; and [8]. However, there is still a lack of stochastic models that incorporate the failure criterion based on EPFM and account for the general nonstationary and non-Gaussian characteristics of related variables. For example, the residual resistance model [9], developed to evaluate the failure of corroded steel pipes, requires three-dimensional characteristics of corrosion pits. Although this information can be obtained using specialised inspection tools, such as 'pigs', the associated computational cost is considerable. To overcome this limitation [10], developed a total in-plane stress model based on the mean and standard deviation of dependent variables. However, its accuracy and efficiency are affected by the linearity and Gaussianity of limit state functions since its solution is based on the second-moment method. Therefore, this model is not available for highly nonlinear or/and non-Gaussian stochastic processes. Further [11], developed a residual strength model, in which the remaining pipe strength is characterised by a lognormal distribution. However, this model does not consider the effects of the corrosion-pitting rate, a factor that introduces considerable uncertainties and exerts a substantial influence on the evaluation of corrosion-induced failure, as demonstrated by Ref. [12].

In this paper, both a fracture toughness-based model and a stress-based model are employed to evaluate the corrosion-induced fracture failure of steel pipes subjected to longitudinal damage. The initial fracture toughness of four grades of mild steel pipes is determined by a new and simple test method [13]. Additionally, the nonstationary and non-Gaussian properties of material properties (e.g., yield stress $\sigma_{ys}(t)$ and ultimate stress $\sigma_{ut}(t)$) and load effects (e.g., internal pressure $P(t)$) are considered when assessing the fracture failure probability of corroded steel pipes. Moreover, the variables that exert significant influence on fracture failure are identified. The primary contribution of this paper is developing an analytical prediction framework for the failure probability of corroded steel pipes, considering the nonstationary and non-Gaussian properties of variables alongside Elastic-Plastic Fracture Mechanics (EPFM). Furthermore, the developed method can contribute to the further application of ductile fracture criteria in the time-dependent assessment of structural integrity. The significance of this paper is that it can provide theoretical evidence for pipe engineers to develop maintenance or repair strategies for steel pipes.

2. Corr oded mild steel pipes

As illustrated in Fig. 1, a corroded steel pipe with an external surface damage is subjected to an internal pressure $P(t)$. The corrosion pit is idealized as semi-elliptical, in which both the corrosion pit depth $a(t)$ and length $2c(t)$ are time dependent. Stochastic models used to predict the pipe failures is commonly based on historical data containing

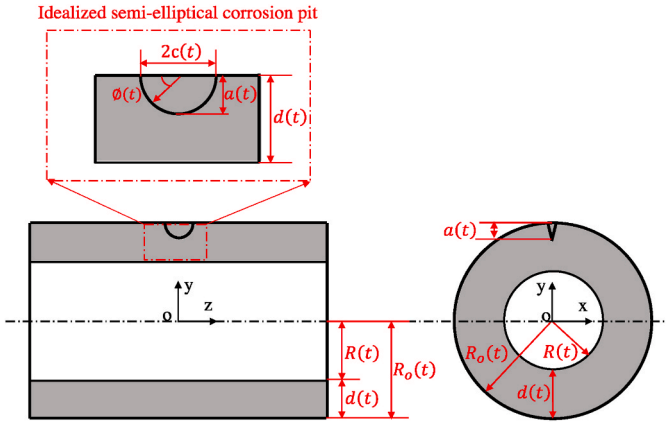

Fig. 1. Illustration of corrosion-induced pipe failure with external surface damage.

various correlated variables [14], including pipe-intrinsic (e.g., pipe age, diameter, length, and materials), environmental (e.g., soil types, precipitation, seasonality, and chemical substances), and operational (e.g., internal pressure, pH values, and maintenance practices). The main variables causing pipe failure are pipe diameter, age, internal pressure, material, and wall thickness [1]. While certain variables remain predominantly static, others are time-dependent, e.g., precipitation and internal pressure [15]. Besides, there is a deterministic relationship between the structural response and these variables. Although some studies have been conducted for assessing the failure probability of steel pipes by time-dependent reliability methods, they are mainly focus on discrete processes, e.g., Weibull and Poisson distributions [16–18]. In this paper, continuous characteristics of stochastic processes are considered.

The corrosion-induced reduction in pipeline wall thickness $d(t)$ can exhibit uniform or localized patterns. Contrary to the common assumption of a constant rate of thickness loss throughout the service life, it usually follows a nonlinear trajectory. Specifically, the corrosion rate is initially high and then experiences a gradual decrease or stabilization. In this research, a power-law relationship proposed by Ref. [19] was employed to describe the corrosion pit depth $a(t)$ as follows:

$$a(t) = k(t)t^{\gamma(t)} \tag{1}$$

where $k(t)$ represents multiplying constant and $\gamma(t)$ represents exponential constant. For the corrosion of steel in soil conditions, $k(t)$ and $\gamma(t)$ have the mean values of 0.3 and 0.6, and coefficients of variation of 0.3 and 0.2, respectively [10].

The internal pressure $P(t)$ was modelled as a Gumbel process [20,21]. Its mean and variance can be expressed as $E[P(t)] = \lambda(t)+0.5772\xi(t)$ and $Var[P(t)] = \frac{\pi^2}{6}\xi^2(t)$, in which $\xi(t)$ and $\lambda(t)$ are scale and location parameters, respectively. The third and fourth moments of the Gumbel process $P(t)$ are $\alpha_{3P}(t)= 1.139$ and $\alpha_{4P}(t)= 5.4$, respectively. The correlation coefficient function of $P(t)$ is assumed as $\rho_P(t_i, t_j) = exp[-((t_i - t_j)/L_P)^2]$, where t_i and t_j are any two time points and L_P represents the correlation length.

Additionally, the yield stress $\sigma_{ys}(t)$ and ultimate stress $\sigma_{us}(t)$ can be modelled as Lognormal processes with the correlation of coefficients being 0.07 and 0.05, respectively [20,21]. The inner radius $R(t)$ and wall thickness $d(t)$ of a pipe can be modelled as normal processes with the correlation of coefficients being 0.001 and 0.015, respectively [20–23]. The related variables and their probabilistic distributions are presented in Table 1. It should be noted that the yield stress $\sigma_{ys}(t)$ and ultimate stress $\sigma_{us}(t)$ presented in Table 1 are the mechanical properties of grade G250 steel. The corresponding mechanical properties for other three grades of mild steel (i.e., G350, PT460NR and A516-70) studied in this study are provided in Table 2.

3. Analytical time-dependent reliability method

In the assessment of pipe failures, a failure criterion should be established first. Based on the time-dependent reliability theory, this criterion can be expressed in the form of a limit state function $G[\boldsymbol{X}(t)]$ as follows:

Table 1
Probabilistic distributions of relevant variables.

Symbol	Mean	Standard deviation	Distribution
$P(t)$ (MPa)	$17.31 + 0.5772*(0.2* t^{0.1})$	$1.2825*(0.2* t^{0.1})$	Gumbel
$\sigma_{ys}(t)$ (MPa)	336	23.52	Lognormal
$\sigma_{us}(t)$ (MPa)	447	22.35	Lognormal
$R(t)$ (mm)	188	0.188	Normal
$d(t)$ (mm)	12	0.18	Normal
$k(t)$	0.30	0.30	Normal
$\gamma(t)$	0.60	0.20	Normal

Table 2
Mechanical and fracture parameters of mild steels [13].

Steel grade	E (GPa)	σ_{ys} (MPa)	ε_{ys} ($\times 10^{-3}$)	σ_{us} (MPa)	n	α	δ_{Ic} (mm)
G250	208	336	9.822	447	6.65	6.08	0.674
G350	207	333	9.549	437	7.30	5.85	0.540
PT460NR	204	401	11.363	521	6.67	5.91	0.577
A516-70	209	398	11.608	543	5.45	6.05	0.736

$$G[\boldsymbol{X}(t)] = G[L, a_L, t] = a_L(t) - L(t) \tag{2}$$

where $L(t)$ denotes the load effect or structural response at time t, $a_L(t)$ denotes an acceptable barrier or structural resistance at time t. Thus, the probability of structural failure $p_f(t)$ can be written in the form of limit state function $G[\boldsymbol{X}(t)]$ as follows:

$$p_f(t) = P\{G[\boldsymbol{X}(t)] \le 0\} = P[L(t) \ge a_L(t)] \tag{3}$$

Equation (3) is a typical upcrossing (outcrossing) problem, which is known as first passage probability. In this theory, only the first upcrossing event is relevant to the structural failure, and the structure is seen as failure when the first upcrossing event occurs, i.e., $G[\boldsymbol{X}(t)] \le 0$. There is an upper bound for $p_f(t)$, which can be written as follows [24,25]:

$$p_f(t) \le p_f(0) + \int_0^T \nu(t)dt \tag{4}$$

where $p_f(0)$ denotes the (instantaneous) probability of failure at time $t = 0$, which can be solved by classical time-independent methods, e.g., First-Order Reliability Method (FORM)/Second-Order Reliability Method (SORM), and $\nu(t)$ represents the outcrossing rate.

The key step in determining the probability of failure $p_f(t)$ is to calculate the outcrossing rate $\nu(t)$. An analytical method [26]; Zhang et al., 2023(b)), named PHI2++ method, is employed in this paper to calculate $\nu(t)$. Based on the theory of a two-component parallel system model [27], if the probability of more than one outcrossing event occurred in $[t, t+\Delta t]$ is considered negligible when $\Delta t \to 0$, the outcrossing rate $\upsilon(t)$ can be defined as follows

$$\upsilon(t) = \lim_{\Delta t \to 0} \frac{P[G[\boldsymbol{X}(t)] > 0 \cap G[\boldsymbol{X}(t+\Delta t)] \le 0]}{\Delta t} \tag{5}$$

Then, based on the FORM, Equation (5) can be written as follows [28]:

$$\upsilon(t) = \lim_{\Delta t \to 0} \frac{\Phi_2\left[\beta_{H-M}(t), -\beta_{H-M}(t+\Delta t), \rho_{\beta_{H-M}}(t, t+\Delta t)\right]}{\Delta t} \tag{6}$$

where $\Phi_2[]$ is the bivariate cumulative normal distribution function, $\beta_{H-M}(t)$ is the high order moments-based reliability indexes, and $\rho_{\beta_{H-M}}(t, t+\Delta t)$ is the correlation coefficient function between $\beta_{H-M}(t)$ and $\beta_{H-M}(t+\Delta t)$.

Since the limit state function $G[\boldsymbol{X}(t)]$ cannot satisfy the requirements $G[\boldsymbol{X}(t)] > 0$ and $G[\boldsymbol{X}(t+\Delta t)] \le 0$ at the same time when $\Delta t = 0$, thus $\lim_{\Delta t \to 0} P[] = 0$, i.e., $\lim_{\Delta t \to 0} \Phi_2[\beta_{H-M}(t), -\beta_{H-M}(t+\Delta t), \rho_{\beta_{H-M}}(t, t+\Delta t)] = 0$. Therefore, when Δt is close to zero, Equation (6) is a limit of indeterminate form, i.e., $\lim_{\Delta t \to 0} 0/0$. Besides, $\lim_{\Delta t \to 0} \frac{\partial \Phi_2[\beta_{H-M}(t), -\beta_{H-M}(t+\Delta t), \rho_{\beta_{H-M}}(t, t+\Delta t)]/\partial \Delta t}{\partial \Delta t / \partial \Delta t}$ exist when $\Delta t \neq 0$. Thus, based on the L'Hopital's rule [29], $\upsilon(t)$ in Equation (6) can be re-written as follows:

$$\upsilon(t) = \lim_{\Delta t \to 0} \frac{\partial \Phi_2\left[\beta_{H-M}(t), -\beta_{H-M}(t+\Delta t), \rho_{\beta_{H-M}}(t, t+\Delta t)\right]}{\partial \Delta t} \tag{7}$$

According to Ref. [28]; $\Phi_2[x, y, \rho]$ has the mathematical properties as follows:

$$\frac{\partial \Phi_2[x, y, \rho]}{\partial y} = \varnothing[y] \Phi\left[\frac{x - \rho y}{\sqrt{1-\rho^2}}\right] \tag{8a}$$

$$\frac{\partial \Phi_2[x, y, \rho]}{\partial \rho} = \frac{\partial^2 \Phi_2[x, y, \rho]}{\partial x \partial y} = \frac{1}{\sqrt{1-\rho^2}} \varnothing[y] \varnothing\left[\frac{x - \rho y}{\sqrt{1-\rho^2}}\right] \tag{8b}$$

where $\varnothing[]$ and $\Phi[]$ are standard normal probability density function and cumulative distribution function, respectively. Thus, based on Equations (8a-b), the outcrossing rate $\upsilon(t)$ in Equation (6) can be further expressed as follows [26]; Zhang et al., 2023(b)):

$$\begin{aligned}
\upsilon(t) = & -\varnothing[\beta_{H-M}(t)] \frac{\partial[\beta_{H-M}(t)]}{\partial t} \Phi\left[-\frac{\frac{\partial[\beta_{H-M}(t)]}{\partial t}}{\sqrt{\frac{\partial^2 \rho_{\beta_{H-M}}(t,t)}{\partial t^2}}}\right] \\
& + \varnothing[\beta_{H-M}(t)] \sqrt{\frac{\partial^2 \rho_{\beta_{H-M}}(t,t)}{\partial t^2}} \varnothing\left[\frac{\frac{\partial[\beta_{H-M}(t)]}{\partial t}}{\sqrt{\frac{\partial^2 \rho_{\beta_{H-M}}(t,t)}{\partial t^2}}}\right] \\
= & \sqrt{\frac{\partial^2 \rho_{\beta_{H-M}}(t,t)}{\partial t^2}} \varnothing[\beta_{H-M}(t)] \left\{ \varnothing\left[\frac{\frac{\partial[\beta_{H-M}(t)]}{\partial t}}{\sqrt{\frac{\partial^2 \rho_{\beta_{H-M}}(t,t)}{\partial t^2}}}\right] - \frac{\frac{\partial[\beta_{H-M}(t)]}{\partial t}}{\sqrt{\frac{\partial^2 \rho_{\beta_{H-M}}(t,t)}{\partial t^2}}} \Phi\left[-\frac{\frac{\partial[\beta_{H-M}(t)]}{\partial t}}{\sqrt{\frac{\partial^2 \rho_{\beta_{H-M}}(t,t)}{\partial t^2}}}\right] \right\}
\end{aligned}$$

Table 3
Summary of all scenarios for $\beta_{H-M}(t)$ [26,30].

$E(t)$	$\alpha_{3Z}(t)$	$\alpha_{4Z}(t)$	$\beta_{H-M}(t)$	$\beta_2(t)$
$(0, +\infty)$	$(-\infty, +\infty)$	$\left(\frac{9+4\alpha_{3Z}^2(t)}{3}, 48\right)$	$\beta_{H-M}^{(1)}(t)$	$(-\infty, +\infty)$
$(-\infty, 0)$	$(0, +\infty)$		$\beta_{H-M}^{(4)}(t)$	$(-P_2(t), -P_1(t))$
			$\beta_{H-M}^{(1)}(t)$	$(-P_2(t), +\infty)$
	$(-\infty, 0)$		$\beta_{H-M}^{(3)}(t)$	$(-P_2(t), -P_1(t))$
			$\beta_{H-M}^{(1)}(t)$	$(-\infty, -P_1(t))$
	$(-\infty, +\infty)$	$\left[\frac{5+4\alpha_{3Z}^2(t)}{3}, \frac{9+4\alpha_{3Z}^2(t)}{3}\right]$	$\beta_{H-M}^{(2)}(t)$	$(-P_1(t), -P_2(t))$

Table 4
Summary of all scenarios for $\rho_{\beta_{H-M}}(t, t+\Delta t)$ [26]; Zhang et al., 2023(b)).

$\boldsymbol{O}(t, t+\Delta t)$	$\boldsymbol{h}_3(t)\boldsymbol{h}_3(t+\Delta t)$	$\boldsymbol{h}_4(t)\boldsymbol{h}_4(t+\Delta t)$	$\boldsymbol{\rho}_{\beta_{H-M}}(t, t+\Delta t)$
$(0, +\infty)$	$(-\infty, +\infty)$	$(0, +\infty)$	$\rho^{(1)}_{\beta_{H-M}}(t, t+\Delta t)$
$(-\infty, 0)$	$(0, +\infty)$		$\rho^{(4)}_{\beta_{H-M}}(t, t+\Delta t)$
			$\rho^{(1)}_{\beta_{H-M}}(t, t+\Delta t)$
	$(-\infty, 0)$		$\rho^{(3)}_{\beta_{H-M}}(t, t+\Delta t)$
			$\rho^{(1)}_{\beta_{H-M}}(t, t+\Delta t)$
	$(-\infty, +\infty)$	$(-\infty, 0)$	$\rho^{(2)}_{\beta_{H-M}}(t, t+\Delta t)$

$$= \sqrt{\frac{\partial^2 \rho_{\beta_{H-M}}(t,t)}{\partial t^2}} \varnothing[\beta_{H-M}(t)] \Psi[x(t)] \tag{9}$$

where $\Psi[x(t)] = \varnothing[x(t)] - x(t)\Phi[-x(t)]$ with $x(t) = \frac{\partial[\beta_{H-M}(t)]}{\partial t} / \sqrt{\frac{\partial^2 \rho_{\beta_{H-M}}(t,t)}{\partial t^2}}$, $\beta_{H-M}(t)$ is high order moments-based reliability index which can be determined from Table 3, and $\rho_{\beta_{H-M}}(t, t)$ is autocorrelation coefficient function which can be determined from Table 4. Determination of related parameters in Tables 3 and 4 is summarized in Appendix I.

4. Applications and analysis

In this section, the failure probability of corrosion-induced mild steel pipes is assessed by the analytical time-dependent reliability method illustrated in Section 3. Four grades of mild steel, i.e., G250, G350, PT460NR and A516-70, are employed in this study. The related mechanical properties and fracture toughness parameters of these mild steel are obtained by the traditional tensile test and the developed new fracture toughness test, respectively. A fracture toughness-based and a stress-based stochastic model is employed in the worked example 1 and 2, respectively. Additionally, the effects of material properties, wall thickness, and internal pressure on the evaluation of fracture failure probability are analysed and discussed.

4.1. Worked example 1

4.1.1. Description of the problem

For ductile materials, such as mild steels, plastic deformation occurs around the crack tip, and material resistance increases as the crack propagates. As a result, EPFM-based parameters, such as J-integral and crack tip opening displacement (δ), should be employed to characterize the fracture behaviour of ductile materials. The J-integral is a measure of the energy required to propagate a crack in a material and is used to characterize the resistance to crack growth [31]. It considers both the elastic and plastic deformations around the crack tip and provides a more comprehensive assessment of the fracture toughness of ductile materials, particularly in the presence of plastic deformation [32]. Furthermore, the fracture behaviours of ductile materials predicted by δ-based criteria exhibit a strong agreement with experimental observations [33].

In the fracture mechanics, fracture failure is considered to occur when the fracture driving force exceeds the fracture resistance [34]. Thus, in the context of crack tip opening displacement (δ), the criterion of fracture failure for corroded steel pipe can be expressed as follows:

$$\delta(t) \geq \delta_R(t) \tag{10}$$

where $\delta(t)$ is the fracture driving force represented by crack tip opening displacement and $\delta_R(t)$ is the fracture resistance represented by acceptable crack tip opening displacement.

Based on Equation (10), fracture failure occurs when $\delta(t) \geq \delta_R(t)$. The probability of corroded mild pipe failure $p_f(t)$ can be determined from Equation (3) with fracture driving force $\delta(t)$ replacing $L(t)$ and fracture resistance $\delta_R(t)$ replacing $a_L(t)$, which are determined below.

4.1.1.1. Fracture driving force $\delta(t)$.

There is a relationship between J-integral and crack tip opening displacement (δ) as follows [35–37]:

$$\delta(t) = \frac{J(t)}{m(t)\sigma_Y(t)} \tag{11}$$

where $\sigma_Y(t)$ is the effective yield stress (i.e., an average of yield stress $\sigma_{ys}(t)$ and ultimate stress $\sigma_{us}(t)$), and $m(t)$ represents a plastic constraint factor. When the ratio of yield stress to ultimate stress is greater than or equal to 0.5, i.e., $\sigma_{ys}(t)/\sigma_{us}(t) \geq 0.5$, the value of $m(t)$ can be determined as follows [38]:

$$m(t) = A_0 - A_1\frac{\sigma_{ys}(t)}{\sigma_{us}(t)} + A_2\left[\frac{\sigma_{ys}(t)}{\sigma_{us}(t)}\right]^2 - A_3\left[\frac{\sigma_{ys}(t)}{\sigma_{us}(t)}\right]^3 \tag{12}$$

where $A_0 = 3.62$, $A_1 = 4.21$, $A_2 = 4.33$ and $A_3 = 2.00$ for the CT specimens.

$J(t)$ can be expressed as a sum of an elastic part $J_{el}(t)$ and plastic part $J_{pl}(t)$ as follows [39]:

$$J(t) = J_{el}(t) + J_{pl}(t) \tag{13}$$

with

$$J_{el}(t) = \frac{K^2(t)}{E'} \tag{14}$$

where $K(t)$ represents stress intensity factor and E' denotes effective elastic modulus, e.g., $E' = E$ for plane stress condition and $E' = E/(1-\nu^2)$ for plane strain condition.

In current practice, the initial fracture toughness under the mode-I loading conditions is widely employed to quantitatively evaluate the material resistance to fracture initiation and the subsequent crack propagation in the failure assessments of engineering structures [40]. Therefore, the stress intensity factor under the mode-I loading conditions, denoted as K_I, is employed in this research. One typical failure case of corroded pipes is caused by internal pressure with external surface damage [7,41]. In this case, the stress intensity factor K_I at any point of a semi-elliptical corrosion pit can be expressed as follows [42]:

$$K_I(t) = \sigma_s(t)\sqrt{\pi\frac{a(t)}{Q(t)}}g\left[\frac{a(t)}{c(t)}, \frac{a(t)}{d(t)}, \frac{d(t)}{R(t)}, \varnothing(t)\right] \tag{15}$$

$$Q(t) = 1 + 1.464\left[\frac{a(t)}{c(t)}\right]^{1.65} \tag{16}$$

where $\sigma_s(t)$ represents the applied stress, $a(t)$ is the depth of pit, $c(t)$ is half-length of pit, $d(t)$ is the wall thickness of pipe, $R(t)$ is the inner radius of pipe, $\varnothing(t)$ is the parametric angle of semi-elliptical pit with $0 \leq \varnothing(t) \leq \pi$, $Q(t)$ is the shape factor for semi-elliptical pit, and $g[]$ is the influence coefficient which can be determined as Appendix II. As the fracture failure of corroded pipe is caused by internal pressure, the applied stress $\sigma_s(t)$ can be expressed by Barlow's formula as follows [12]:

$$\sigma_s(t) = \sigma_{hoop}(t) = P(t)R_0(t)/d(t) \tag{17}$$

where $\sigma_{hoop}(t)$ represents the hoop stress, $P(t)$ is the internal pressure, and $R_0(t)$ is the outer radius of pipe. Hoop stress can lead to the fracture of pipe with a longitudinal defect or damage, which is a main reason of pipe failure.

The plastic part $J_{pl}(t)$ can be expressed as follows [43]:

$$J_{pl}(t) = \alpha\varepsilon_0\sigma_0 L(t)h\left[\frac{2\varnothing(t)}{\pi}, \frac{a(t)}{c(t)}, \frac{a(t)}{d(t)}, \frac{d(t)}{R(t)}, n\right]\left[\frac{P(t)}{P_0(t)}\right]^{n+1} \tag{18}$$

where α and n represent the multiplying and exponential constant in the Ramberg–Osgood model, σ_0 denotes reference stress which is usually determined as yield stress, i.e., $\sigma_0 = \sigma_{ys}$, ε_0 represents the strain ac-

cording to the reference stress σ_0, $L(t)$ represents the characteristic length of pipe, i.e., $L(t) = 2c(t)$, $P_0(t)$ represents the limit pressure under the fully plastic condition (i.e., $n = \infty$), which can be determined from $P_0(t) = \sigma_0 d(t)/R(t)$, and $h(t)$ represents the normalised fully plastic J-integral, which can be determined as Appendix II.

Thus, $J(t)$ (i.e., in Equation (13)) can be determined as follows:

$$J(t) = \frac{\pi}{E}\frac{a(t)}{Q(t)}\sigma_s^2(t)g^2(t) + \alpha\varepsilon_0\sigma_0 L(t)h(t)\left[\frac{P(t)}{P_0(t)}\right]^{n+1} \tag{19}$$

Furthermore, based on Equation (11), Equation (19) can be determined as follows:

$$\delta(t) = \frac{\pi}{E}\frac{a(t)}{Q(t)}\frac{\sigma_s^2(t)g^2(t)}{m(t)\sigma_Y(t)} + \alpha\varepsilon_0\sigma_0\frac{L(t)h(t)}{m(t)\sigma_Y(t)}\left[\frac{P(t)}{P_0(t)}\right]^{n+1} \tag{20}$$

where $m(t)$, $g(t)$, $\sigma_s(t)$ and $h(t)$ are determined from Equation (12), (A2.1), (17) and (A2.2), respectively.

4.1.1.2. Fracture resistance $\delta_R(t)$. Fracture toughness is a critical property of ductile materials, which can be used to measure the fracture resistance to crack propagation. It is crucial in assessing the ability of a material to withstand crack initiation and growth under various loading conditions [44]. The initial fracture toughness is often employed in evaluating structural performance and quality assurance of engineering components [40].

In this paper, a new and simple test method (Zhang et al., 2023(a)) is employed for determining the initial fracture toughness of four grades of mild steel, i.e., G250, G350, PT46NT and A516-70. Based on this newly developed test method, the initial fracture toughness can be determined solely by the mechanical properties obtained from tensile tests. Specifically, this method is developed based on an established correlation between critical strain energy density and initial fracture toughness. There is a constant relationship between the crack tip opening displacement at fracture initiation (δ_{ic}) and the average elongation length (l_c), i.e., $\delta_{ic} = R_c l_c$. $R_c = 3.068$ and l_c can determined from tensile tests. Additionally, the accuracy of this method has been verified by both unloading compliance (UC) method and developed Digital Image Correction (DIC) technique-based method. For example, there is a high level of agreement between the initial fracture toughness values obtained from the proposed method and the DIC-based tests, i.e., less than 5 % in the deviation value.

The critical value of fracture resistance, i.e., δ_{Ic}, is obtained as shown in Table 2, which will be used as the critical barrier for assessing the failure probability of corroded steel pipes. Besides, the mechanical parameters required for determining the driving force $\delta(t)$ are also presented in Table 2.

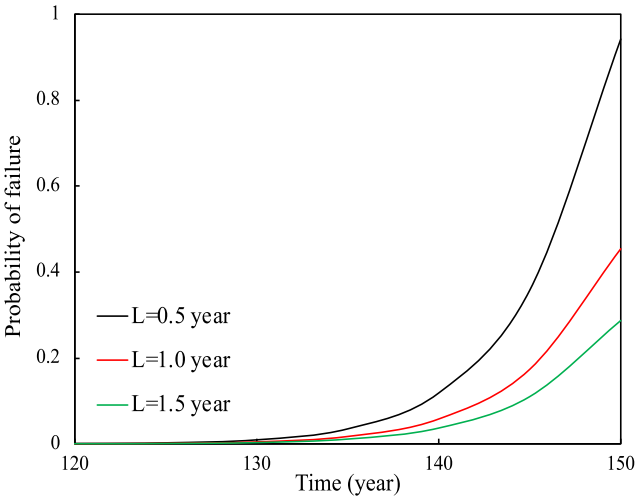

Fig. 3. Effect of correlation lengths on the probability of failure of worked example 1.

4.1.2. Results and analysis

In this Section, based on the probabilistic distributions of variables provided in Tables 1 and 2, PHI2++ method [26]; Zhang et al., 2023(b)) is employed to calculate the outcrossing rate for four grades of mild steel (G250, G350, PT46NR, and A516-70). Since the accuracy and efficiency of PHI2++ method have been thoroughly verified by different approaches in Ref. [26]; Zhang et al., 2023(b)), this paper does not repeat the verification process. Additionally, the influences of correlation lengths of stochastic process on the determination of probability of failure $p_f(t)$ are studied.

The obtained results of probability of failure $p_f(t)$ are presented in Fig. 2. Based on Fig. 2(a), it was found that the probability of failure of G250 steel is lower than that of G350 steel. Since the initial fracture toughness $\delta_{Ic}(t)$ (i.e., fracture resistance) of G250 steel is larger than that of G350, thus, it has less probability of fracture failure than G350 steel. It was also found that the both the probability of failure $p_f(t)$ of PT460NR and A516-70 steel are much smaller than those of G250 and G350 steel.

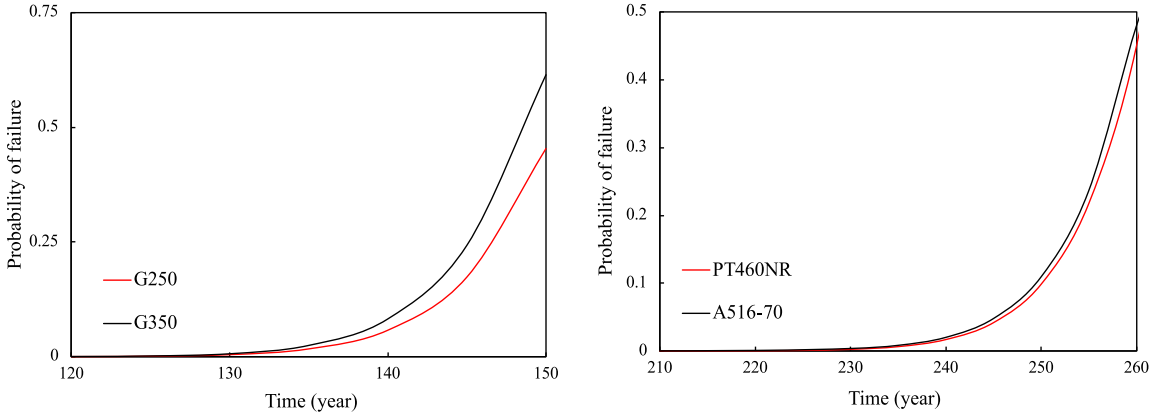

Fig. 2. Probability of failure of worked example 1: (a) G250 and G350 steel and (b) PT460NR and A516-70 steel.

For example, when the time equals to 150 years, the failure probability of G250 and G350 steel are 0.453 and 0.614, respectively. However, these values of PT460NR and A516-70 steel are nearly equal to zero. Both PT460NR and A516-70 are not only mild steel but also boiler plate steel, typically used in the construction of boilers and high-pressure vessels. Therefore, boiler plate steel exhibits a remarkable capacity to withstand high-pressure in pipeline applications, while maintaining a low probability of failure. As shown in Table 2, compared with G250 and G350 steel, both PT460NR and A516-70 steel exhibit a substantially higher yield stress and ultimate stress, which make them can endure a high level of hoop stress. This observation suggests that stress has a significant role in the assessment of structure reliability of mild steel. Consequently, the reliability evaluation of mild steel necessitates a comprehensive criterion, such as combining initial fracture toughness with ultimate stress, rather than relies solely on one parameter.

Furthermore, to investigate the impacts of the bandwidth of stochastic process on the probability of failure, it is crucial to consider the correlation lengths. In order to assess this, the correlation length (L_P) of the internal pressure $P(t)$ was set to three distinct values: 0.5, 1.0, and 1.5 years. The corresponding results are presented in Fig. 3. It is observed that as the correlation length increases (i.e., transitioning from 0.5 to 1.0 and 1.5 years), there is a noticeable decrease in the probability of failure. This decrease can be attributed to the widening of the bandwidth of stochastic process. With an increase in the correlation length, the bandwidth decreases, resulting in reduced correlation among outcrossing events. Consequently, the occurrence probability of outcrossing decreases with lower probability of failure.

4.1.3. Sensitivity analysis

In this section, the effects of radius, wall thickness and material properties on the calculation of failure probability are analysed. To study the effects of wall thickness on the calculation of probability of failure $p_f(t)$, the mean value of original wall thickness, denoted as $d(t)$, is systematically reduced to 0.98* $d(t)$, 0.96* $d(t)$, 0.94* $d(t)$ and 0.92* $d(t)$. The resulting probability of failure $p_f(t)$ is presented in Fig. 4(a). It can be seen that $p_f(t)$ experiences a substantial increase as the wall thickness decreases, which is consistent with the research findings reported by Refs. [45,46]. Similarly, to investigate the effects of internal pressure, the mean value of internal pressure $P(t)$ is systematically increased to $P(t)/0.98$, $P(t)/0.96$, $P(t)/0.94$ and $P(t)/0.92$. The corresponding results are illustrated in Fig. 4(b). It was found that the probability of failure significantly increases with increasing of internal pressure. It makes sense that the increase of internal pressure will result in a higher fracture driving force $\delta(t)$, as illustrated in Equation (20), which leads to an increase in probability of failure.

It is important to note that the changes in the radius of a pipe does not necessarily correspond to proportional changes in the wall thickness. Therefore, it is better to study the ratio effect of wall thickness to inner radius, i.e., $d(t)/R(t)$, on the evaluation of probability of failure $p_f(t)$. Furthermore, to make a comparison of effects between the $d(t)/R(t)$ and internal pressure $P(t)$ on the evaluation of probability of failure $p_f(t)$, a

Table 5
Effect of $d(t)/R(t)$ on the probability of failure of worked example 1.

Wall thickness $d(t)$ (mm)	$d(t)/R(t)$ ($\times 10^{-2}$)	$d(t)/R(t)$ reduced (%)	Time (year)	Time reduced (%)
$d(t)$	6.383	0	149.052	0
0.98* $d(t)$	6.255	2.0	134.555	9.726
0.96* $d(t)$	6.128	4.0	120.625	19.072
0.94* $d(t)$	6.000	6.0	107.257	28.041
0.92* $d(t)$	5.872	8.0	95.283	36.074

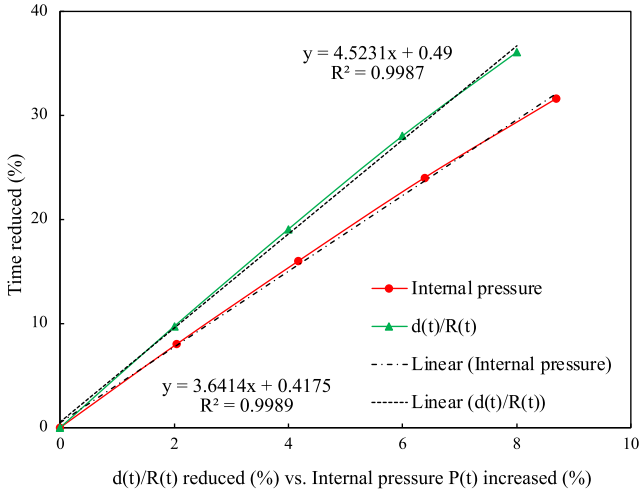

Fig. 5. Effect comparison of $d(t)/R(t)$ and internal pressure on the probability of failure of worked example 1.

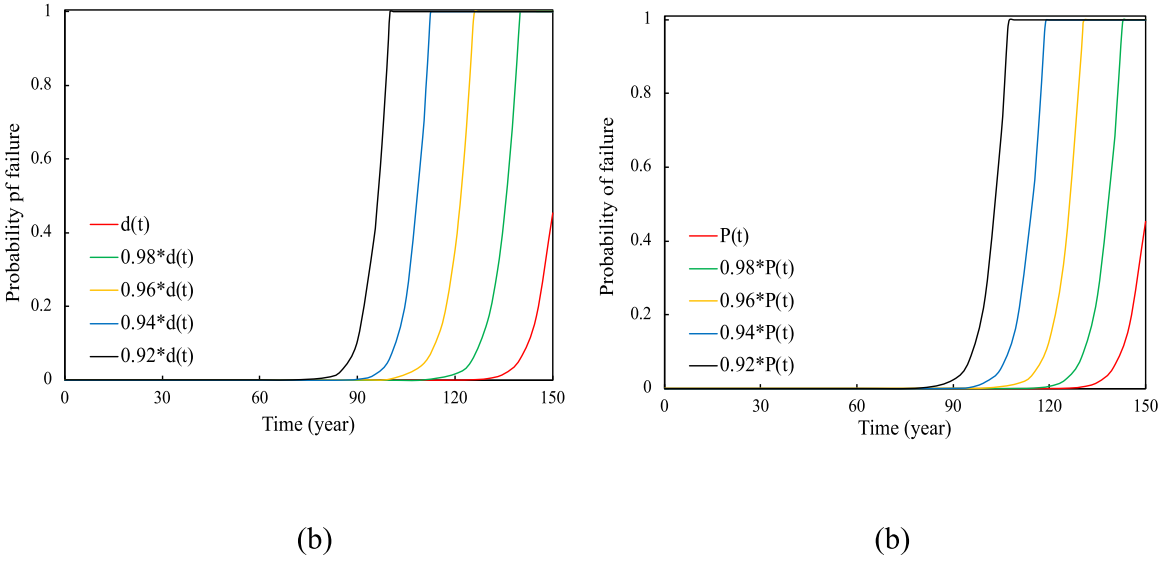

(b) (b)

Fig. 4. Sensitivity analysis on the probability of failure of worked example 1: (a) wall thickness and (b) internal pressure.

Table 6
Effect of internal pressure on the probability of failure of worked example 1.

Internal pressure $P(t)$ (MPa)	$P(t)$ increased (%)	Time (year)	Time reduced (%)
$P(t)$	0	149.052	0
$P(t)/0.98$	2.041	137.101	8.018
$P(t)/0.96$	4.167	125.243	15.974
$P(t)/0.94$	6.383	113.290	23.993
$P(t)/0.92$	8.696	101.930	31.614

detailed (mathematical) relationship between $d(t)/R(t)$ and $p_f(t)$ as well as $P(t)$ and $p_f(t)$ should be studied. Based on the results presented in Fig. 4(a), the reduced ratios of wall thickness $d(t)$ to inner radius of pipe $R(t)$, i.e., $d(t)/R(t)$, are calculated as shown in Table 5. At the same time, reduced time corresponding to the probability of failure with a value of 0.4 are calculated. Subsequently, the relationship between time reduced (i.e., probability of failure increased) and $d(t)/R(t)$ reduced is plotted in Fig. 5. It can be observed that there is a nearly linear relationship between $d(t)/R(t)$ and $p_f(t)$. For example, a reduction of 1.0 % in the ratio $d(t)/R(t)$ will cause an increase of 4.523 % in $p_f(t)$.

Similarly, based on the results presented in Fig. 4(b), the increased internal pressure $P(t)$ and time reduced corresponding to the probability of failure $p_f(t)$ with a value of 0.4 are calculated, as shown in Table 6. Subsequently, the relationship between the internal pressure increased and time reduced (i.e., probability of failure increased) is plotted in Fig. 5. It was found that there is also a nearly linear relationship between $p_f(t)$ and $P(t)$. For instance, an increase of 1.0 % in the $P(t)$ will cause an increase of 3.641 % in $p_f(t)$. Consequently, based on Fig. 5, the ratio of wall thickness to inner radius $d(t)/R(t)$ has a more substantial influence than internal pressure $P(t)$ on the evaluation of $p_f(t)$.

4.2. Worked example 2

4.2.1. Description of the problem

Based on the results of reliability analysis in the worked example 1, initial fracture toughness $\delta_{Ic}(t)$ is not effective enough for evaluating the material resistance to fracture initiation. The limiting (or ultimate) stress also plays an essential role in the assessment of material resistance [10]. Therefore, this section primarily focuses on using the same analytical time-dependent method to evaluate the probability of failure in corroded mild steel pipes, employing the stress-based fracture failure criterion. When assuming that the pipes are uniformly loaded and supported along their length, only the hoop stress is of interest. Hoop stress can cause a longitudinal defect or damage, which is a main reason of pipe failure. Thus, in the context of stress, the fracture failure criterion of corroded steel pipe can be expressed as follows [47]:

$$\sigma_{hoop}(t) \geq \sigma_{us}(t) \tag{21}$$

where $\sigma_{hoop}(t)$ is the fracture driving force represented by hoop stress and $\sigma_{us}(t)$ is the fracture resistance represented by the ultimate stress.

Based on Equation (21), fracture failure occurs when $\sigma_{hoop}(t) \geq \sigma_{us}(t)$. The probability of corroded mild pipe failure $p_f(t)$ can be determined from Equation (3) with fracture driving force $\sigma_{hoop}(t)$ replacing $L(t)$ and fracture resistance $\sigma_{us}(t)$ replacing $a_L(t)$. The hoop stress $\sigma_{hoop}(t)$ can be determined as follows [12]:

$$\sigma_{hoop}(t) = P(t)R_0(t) / d(t) \tag{22}$$

where $P(t)$ is the internal pressure, $R_0(t)$ is the outer radius of pipe, and $d(t)$ is the wall thickness. The probabilistic distributions of $P(t)$, $R_0(t)$, $d(t)$ and $\sigma_{us}(t)$ are presented in Tables 1 and 2

4.2.2. Results and analysis

According to the stress-based fracture failure criterion, i.e., Equation (21), the obtained probability of fracture failure for four grades of mild steel pipes is presented in Fig. 6. The mean values of internal pressure $P(t)$ and wall thickness $d(t)$ are 17.31 + 0.5772*(0.2* $t^{0.1}$) and 12, respectively. The correlation length of $P(t)$ is 1.0 year. According to Fig. 6, it was found that the probability of fracture failure increases with an increase in the ultimate stress.

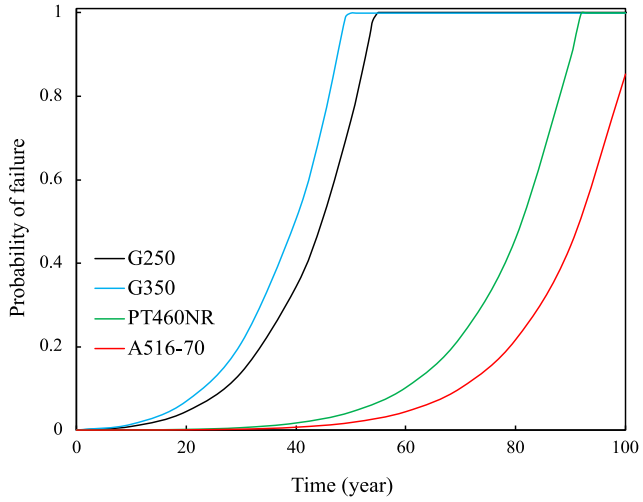

Fig. 6. Comparison of probability of failure among different grades of steel of worked example 2.

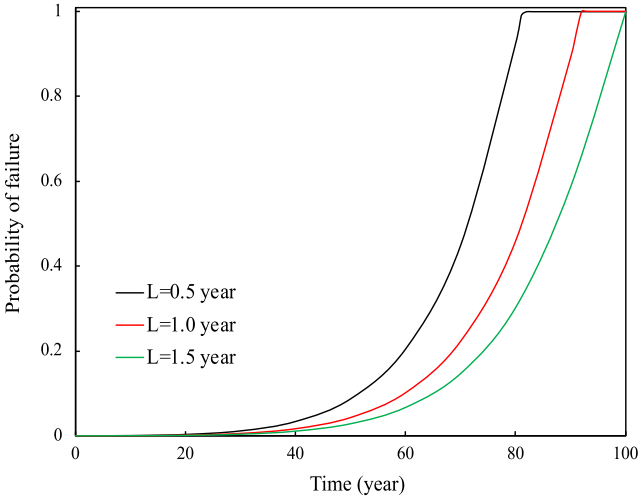

Fig. 7. Effect of correlation lengths on the probability of failure of worked example 2.

Additionally, the impacts of the bandwidth of stochastic process on the probability of failure are studied. Like worked example 1, the correlation length (L_P) of the internal pressure $P(t)$ was set to three distinct values: 0.5, 1.0, and 1.5 years. The corresponding results for the grade PT460NR steel are presented in Fig. 7. It is also observed that there is a noticeable decrease in the probability of failure as the correlation length increases, i.e., transitioning from 0.5 to 1.0 and 1.5 years.

To further investigate the failure criteria regarding the evaluation of fracture failure probability, a comparison is made between the probability of fracture failure obtained from the energy-based (i.e., initial fracture toughness) and the stress-based (i.e., ultimate stress) fracture failure criteria, as shown in Fig. 8. The results indicate that the probability of failure obtained from the stress-based criterion is significantly higher than that obtained from the energy-based criterion. For instance, as shown in Fig. 8(a), the stress-based criterion predicts a failure

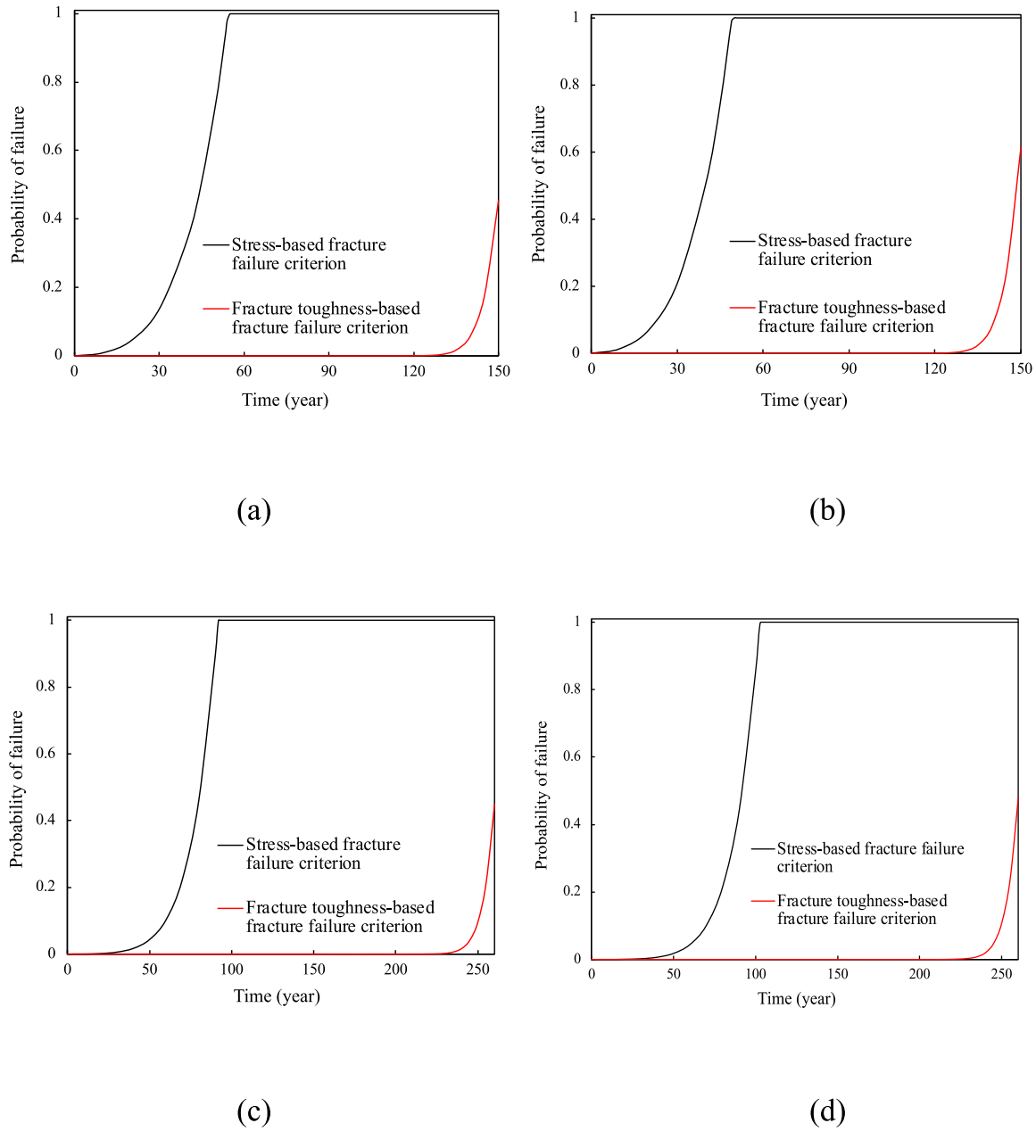

Fig. 8. Comparison of probability of failure between stress-based and fracture toughness-based fracture failure criteria: (a) G250, (b) G350, (3) PT460NR and (4) A516-70.

probability of 1.0 for G250 steel at 60 years, whereas the energy-based criterion indicates a failure probability close to zero. Similarly, in Fig. 8 (c), the stress-based criterion predicts a failure probability of 1.0 at 100 years for PT460NR steel, whereas the energy-based criterion indicates a failure probability close to zero.

Based on the above analysis, the stress-based fracture failure criterion tends to provide a conservative evaluation on the reliability of corroded mild steel pipes. This is because that the effects of strain hardening around the crack tip is not considered. Unlike brittle materials, fracture failure in ductile materials does not occur at the limiting stress, i.e., ultimate stress. Crack tip blunting caused by the strain hardening effect can increase the material resistance to fracture initiation. Therefore, depending solely on the stress-based fracture failure criterion is not sufficiently effective for evaluating the reliability of mild steel pipes.

4.2.3. *Sensitivity analysis*

In this section, according to the stress-based fracture failure criterion, the effects of radius, wall thickness and material properties on the calculation of failure probability are analysed. Like the sensitivity analysis conducted in Section 4.1.3, the mean value of original wall thickness, denoted as $d(t)$, is systematically reduced to 0.98* $d(t)$, 0.96* $d(t)$, 0.94* $d(t)$ and 0.92* $d(t)$ to study the effects of wall thickness $d(t)$ on the calculation of the probability of failure. The calculation results for the grade of PT460NT steel are presented in Fig. 9(a), in which the mean of internal pressure $P(t)$ is $17.31 + 0.5772*(0.2* t^{0.1})$. The results illustrated in Fig. 9(a) indicate that the probability of fracture failure increases as the wall thickness decreases. Additionally, to investigate the effects of internal pressure $P(t)$ on the evaluation of failure probability, the mean value of internal pressure $P(t)$ is systematically increased to $P(t)/0.98$, $P(t)/0.96$, $P(t)/0.94$ and $P(t)/0.92$. The corresponding results for the grade of PT460NR steel are presented in Fig. 9(b), in which the

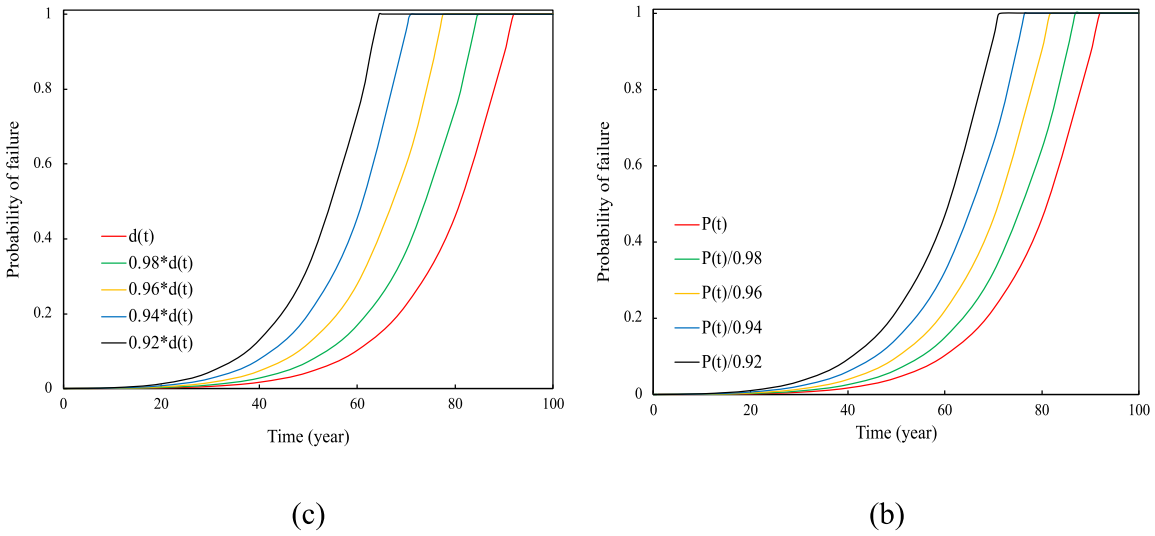

Fig. 9. Sensitivity analysis on the probability of failure of worked example 2: (a) wall thickness and (b) internal pressure.

Table 7
Effect of $d(t)/R(t)$ on the probability of failure of worked example 2.

Wall thickness $d(t)$ (mm)	$d(t)/R(t)$ ($\times 10^{-2}$)	$d(t)/R(t)$ reduced (%)	Time (year)	Time reduced (%)
$d(t)$	6.383	0	78.071	0
0.98* $d(t)$	6.255	2.0	71.078	8.957
0.96* $d(t)$	6.128	4.0	64.312	17.623
0.94* $d(t)$	6.000	6.0	58.437	25.149
0.92* $d(t)$	5.872	8.0	52.187	33.154

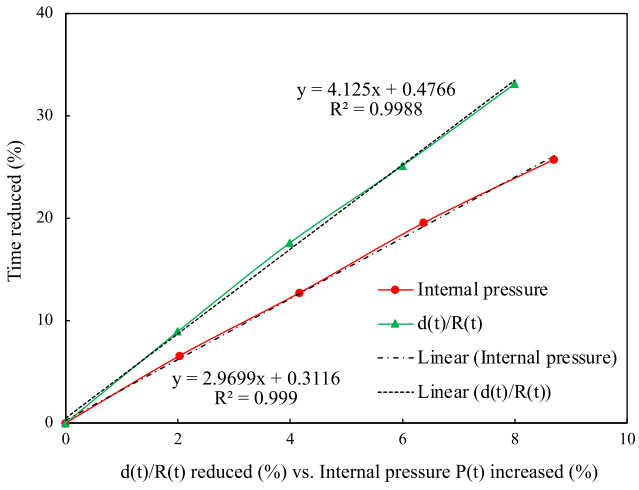

Fig. 10. Effect comparison of $d(t)/R(t)$ and internal pressure on the probability of failure of worked example 2.

Table 8
Effect of internal pressure on the probability of failure of worked example 2.

Internal pressure $P(t)$ (MPa)	$P(t)$ increased (%)	Time (year)	Time reduced (%)
$P(t)$	0	78.072	0
$P(t)/0.98$	2.041	72.907	6.616
$P(t)/0.96$	4.167	68.118	12.750
$P(t)/0.94$	6.383	62.758	19.615
$P(t)/0.92$	8.696	57.933	25.795

mean value of wall thickness is 12 mm. The results illustrated in Fig. 9(b) also show that the probability of fracture failure significantly increases with the increase of internal pressure $P(t)$.

Furthermore, the reduced ratios of wall thickness $d(t)$ to inner radius of pipe $R(t)$, i.e., $d(t)/R(t)$, are calculated based on the results presented in Fig. 9(a). The reduced time corresponding to a probability of failure of 0.4 is calculated and is shown in Table 7. Then, a plot depicting the relationship between the reduction in time and the reduction in $d(t)/R(t)$ is presented in Fig. 10. A nearly linear relationship exists between $d(t)/R(t)$ and the probability of failure. For example, a 1.0 % reduction in the $d(t)/R(t)$ ratio results in a 4.125 % increase in the probability of failure $p_f(t)$.

Similarly, based on the results in Fig. 9(b), the increased internal pressure $P(t)$ and the corresponding reduced time for a probability of failure of 0.4 are calculated and presented in Table 8. Subsequently, the relationship between the internal pressure increased and the time reduced is plotted in Fig. 10. A nearly linear relationship was observed between the probability of failure and internal pressure $P(t)$. For instance, a 1.0 % increase in internal pressure $P(t)$ results in a 2.97 % increase in the probability of failure. Consequently, same as the sensitivity analysis conducted according to the fracture toughness-based fracture failure criterion, the ratio of wall thickness to inner radius $d(t)/R(t)$ has a more essential influence on the evaluation of the probability of failure than the internal pressure $P(t)$.

5. Further discussion

Based on the reliability analysis results of worked example 1 and 2, it is evident that the evaluation of material resistance to fracture initiation in mild steel cannot solely rely on initial fracture toughness or ultimate stress. For example, under the fracture toughness-based criterion, although PT460NR steel exhibits a lower crack tip opening displacement

at fracture initiation compared to G350 steel, its probability of failure is lower due to higher yield and ultimate stress. Furthermore, in comparison to the fracture toughness-based criterion, the stress-based fracture failure criterion tends to provide a conservative evaluation of structural reliability, as it does not consider the strain hardening effects. Therefore, for a comprehensive assessment of material resistance of mild steel structures, a criterion that integrates initial fracture toughness with ultimate stress should be developed.

In general, the fracture failure types of pipes can be classified into three groups, i.e., circumferential fracture, longitudinal fracture, and bell splitting fracture. However, one of limitations in this study is that the employed stochastic model illustrates pipes restricted to the internal water pressure, therefore, only the longitudinal fracture failure type is considered. Although the longitudinal fracture failure is the prominent failure type in both small-diameter and large-diameter pipes [48,49], it is necessary to consider the failure probability caused by other fracture types. Furthermore, the primary component of the fracture driving force is considered to be the hoop stress caused by internal pressure. However, it is important to note that stress generated by other types of loading effects, such as soil weight and traffic loading, which were not considered may also play a significant role in evaluating the fracture failure of mild steel pipes [10]. Therefore, it is necessary to take these loading effects into consideration in the future studies.

In this study, only compact-tension (CT) specimens were used to determine the fracture driving force and material resistance for evaluating the probability of failure. Therefore, it cannot be ensured that the crack tip conditions, such as constraints, stress concentration and plastic deformation, are similar between the CT specimens and full-scale pipes. As such, further investigations involving different types of specimens, e.g., single-edge-bend and single-edge-notch tension, are necessary to enhance the efficiency of stochastic models and the accuracy of failure prediction.

6. Conclusion

In this paper, the corrosion-induced failure of mild steel pipes has been evaluated by an analytical time-dependent reliability method, based on both fracture toughness-based and stress-based stochastic models. The nonstationary and non-Gaussian properties of material properties and load effects are considered for assessing the probability of pipe failure. The effects of correlation lengths of stochastic process on the evaluation of failure probability have been studied. Moreover, the factors affecting the probability of failure are identified and discussed. It has been found that the probability of corrosion-induced pipe failure increases as the correlation lengths of stochastic processes decrease. It has also been found that there is a linear relationship between changes in the ratio of wall thickness $d(t)$ to inner radius $R(t)$ and the probability of failure $p_f(t)$. There is also a linear relationship between changes in the internal pressure $P(t)$ and the probability of failure $p_f(t)$. Furthermore, $d(t)/R(t)$ has been found to play a more significant role in the evaluation of the probability of failure than $P(t)$. Moreover, a comprehensive criterion is necessary for evaluating the material resistance to fracture initiation in corroded mild steel, such as incorporating initial fracture toughness with ultimate stress. The significance of this paper lies in its ability to analytically predict the failure probability of corroded mild steel pipes, considering both nonstationary and non-Gaussian properties of related variables and elastic-plastic fracture mechanics. It can be concluded that the findings can serve as theoretical evidence for pipe engineers to develop maintenance or repair strategies for mild steel pipes.

CRediT authorship contribution statement

Bohua Zhang: Validation, Experiment, Methodology, Investigation, Formal analysis, Data curation, Writing - original draft. **Haoran Lei:** Investigation, Data curation, Investigation, Writing - review & editing. **Xiancun Hu:** Investigation, Formal analysis, Writing - review & editing. **Chun-Qing Li:** Conceptualization, Methodology, Funding acquisition, Project administration, Supervision, Writing - review & editing.

Declaration of competing interest

The authors declare that they have no known competing financial interests or personal relationships that could have appeared to influence the work reported in this paper.

Data availability

Data will be made available on request.

Acknowledgement

The authors gratefully acknowledge the financial support provided by the Australian Research Council through grants DP230100983 and IC230100015.

APPENDIX I

Determination of related parameters in Table 2 is shown as follows [26]; Zhang et al., 2023(b)):

$$\beta_{H-M}^{(1)}(t)=\left[\sqrt{D(t)}-\frac{C(t)}{2}\right]^{1/3}-\left[\sqrt{D(t)}+\frac{C(t)}{2}\right]^{1/3}+\frac{h_3(t)}{3h_4(t)} \tag{A1.1}$$

$$\beta_{H-M}^{(2)}(t)=2\sqrt{-\frac{E(t)}{3}}\cos\left[\frac{\theta(t)+\pi}{3}\right]+\frac{h_3(t)}{3h_4(t)} \tag{A1.2}$$

$$\beta_{H-M}^{(3)}(t)=2\sqrt{-\frac{E(t)}{3}}\cos\left[\frac{\theta(t)-\pi}{3}\right]+\frac{h_3(t)}{3h_4(t)} \tag{A1.3}$$

$$\beta_{H-M}^{(4)}(t)=-2\sqrt{-\frac{E(t)}{3}}\cos\left[\frac{\theta(t)}{3}\right]+\frac{h_3(t)}{3h_4(t)} \tag{A1.4}$$

with

$$C(t)=-\frac{2}{27}\left[\frac{h_3(t)}{h_4(t)}\right]^3+\frac{h_3(t)}{3h_4^2(t)}-\frac{\beta_2(t)}{k(t)h_4(t)} \tag{A1.5a}$$

$$D(t)=\left[\frac{E(t)}{3}\right]^3+\left[\frac{C(t)}{2}\right]^2 \tag{A1.5b}$$

$$\theta(t)=arccos\left\{\frac{-C(t)}{2[-E(t)/3]^{3/2}}\right\} \tag{A1.5c}$$

$$P_1(t)=k(t)h_4(t)\left\{2[-E(t)/3]^{3/2}+\frac{2}{27}\left[\frac{h_3(t)}{3h_4(t)}\right]^3-\frac{h_3(t)}{3h_4^2(t)}\right\} \tag{A1.5d}$$

$$P_2(t)=k(t)h_4(t)\left\{-2[-E(t)/3]^{3/2}+\frac{2}{27}\left[\frac{h_3(t)}{3h_4(t)}\right]^3-\frac{h_3(t)}{3h_4^2(t)}\right\} \tag{A1.5e}$$

Determination of related parameters in Table 3 is shown as follows [26,30]:

$$\rho^{(1)}_{\beta_{H-M}}(t,t+\Delta t)=\left[\sqrt{L(t)}-\frac{J(t)}{2}\right]^{1/3}-\left[\sqrt{L(t)}+\frac{J(t)}{2}\right]^{1/3}-\frac{h_3(t)h_3(t+\Delta t)}{9h_4(t)h_4(t+\Delta t)} \tag{A1.6}$$

$$\rho^{(2)}_{\beta_{H-M}}(t,t+\Delta t)=-2\sqrt{-\frac{O(t)}{3}}\cos\left[\frac{\omega(t)+\pi}{3}\right]-\frac{h_3(t)h_3(t+\Delta t)}{9h_4(t)h_4(t+\Delta t)} \tag{A1.7}$$

$$\rho^{(3)}_{\beta_{H-M}}(t,t+\Delta t)=-2\sqrt{-\frac{O(t)}{3}}\cos\left[\frac{\omega(t)-\pi}{3}\right]-\frac{h_3(t)h_3(t+\Delta t)}{9h_4(t)h_4(t+\Delta t)} \tag{A1.8}$$

$$\rho^{(4)}_{\beta_{H-M}}(t,t+\Delta t)=2\sqrt{-\frac{O(t)}{3}}\cos\left[\frac{\omega(t)}{3}\right]-\frac{h_3(t)h_3(t+\Delta t)}{9h_4(t)h_4(t+\Delta t)} \tag{A1.9}$$

with

$$(J)=\frac{2}{729}\left[\frac{h_3(t)h_3(t+\Delta t)}{h_4(t)h_4(t+\Delta t)}\right]^3-\frac{1}{54}\frac{h_3(t)h_3(t+\Delta t)}{h_4^2(t)h_4^2(t+\Delta t)}-\frac{\rho_Z(t,t+\Delta t)}{6k(t)k(t+\Delta t)h_4(t)h_4(t+\Delta t)} \tag{A1.10a}$$

$$L(t)=\left[\frac{O(t)}{3}\right]^3+\left[\frac{J(t)}{2}\right]^2 \tag{A1.10b}$$

$$\omega(t)=arccos\left\{\frac{-J(t)}{2[-O(t)/3]^{3/2}}\right\} \tag{A1.10c}$$

APPENDIX II

$g[]$ is the influence coefficient which can be determined as follows [47]:

$$g(t)=\left(g_1+g_2\frac{a(t)}{c(t)}+\left\{g_3+g_4\frac{a(t)}{c(t)}+g_5\left[\frac{a(t)}{c(t)}\right]^2\right\}\left[\frac{a(t)}{d(t)}\right]^2+\left\{g_6+g_7\frac{a(t)}{c(t)}+g_8\left[\frac{a(t)}{c(t)}\right]^2\right\}\left[\frac{a(t)}{d(t)}\right]^4\right)exp\left[g_9\frac{d(t)}{R(t)}\right] \tag{A2.1}$$

where $g_i(i=1,2,\ldots,9)$ denotes the coefficients corresponding to the locations along the semi-elliptical corrosion pit. In this study, to obtain a maximum value of $K_I(t)$, the measurement point is selected as the deepest location of pit, i.e., $\varnothing(t)=\pi/2$. Thus, $g_1=0.983$, $g_2=-0.028$, $g_3=2.806$, $g_4=-4.077$, $g_5=1.580$, $g_6=0.000$, $g_7=-1.217$, $g_8=0.776$, and $g_9=0.160$.

$h(t)$ represents the normalised fully plastic $J-$ integral, which can be determined as follows [50]:

$$h(t)=\lambda_1(t)exp\left\{[a(t)/d(t)]\sqrt{[a(t)/d(t)][R(t)/d(t)]}\right\}+\lambda_2(t)exp\left\{\sqrt{3\cos[\beta(t)]}\right\}+\lambda_3(t)exp\left\{[c(t)/a(t)][a(t)/d(t)]^2\cos[\beta(t)]\right\}+\lambda_4(t) \tag{A2.2}$$

with

$$\lambda_1(t)=0.13[d(t)/a(t)]^2\cos[\beta(t)]\sqrt{\cos[\beta(t)]/n} \tag{A2.3a}$$

$$\lambda_2(t)=0.61461\sqrt{c(t)/a(t)} \tag{A2.3b}$$

$$\lambda_3(t)=11.6742n[a(t)/d(t)]^2\{\cos[\beta(t)]\}^2\sqrt{c(t)/a(t)}\sqrt{d(t)/R(t)} \tag{A2.3c}$$

$$\lambda_4(t)=-0.53016 \tag{A2.3d}$$

where $\beta(t)$ is the angle between the damage and pipe axis, with $\beta(t)=0^\circ$ for the longitudinal damage. It should be noted that Equation (18) is valid when $0.025\le d(t)/R(t)\le 0.1$, $0.2\le a(t)/d(t)\le 0.8$, $0.4\le a(t)/c(t)\le 1.5$ and $3\le n\le 10$.

References

[1] R. Taiwo, I.A. Shaban, T. Zayed, Development of sustainable water infrastructure: a proper understanding of water pipe failure, J. Clean. Prod. (2023), 136653.
[2] B. Rajani, S. Tesfamariam, Estimating time to failure of ageing cast iron water mains under uncertainties, ICE Water Manag. J 160 (2) (2005) 83–88.
[3] A. Pękala, K. Pietrucha-Urbanik, The influence of the soil environment on the corrosivity of failure infrastructure-case study of the exemplary water network, Arch. Civ. Eng. 64 (1) (2018).
[4] E. Ana, W. Bauwens, M. Pessemier, C. Thoeye, S. Smolders, I. Boonen, G. De Gueldre, An investigation of the factors influencing sewer structural deterioration, Urban Water J. 6 (4) (2009) 303–312.
[5] G. Kley, N. Caradot, Review of Sewer Deterioration Models, vol. 1, KWB project SEMA, 2013, p. 43. *Report*.
[6] W. Wang, W. Shi, C.Q. Li, Time dependent reliability analysis for cast iron pipes subjected to pitting corrosion, Int. J. Pres. Ves. Pip. 175 (2019), 103935.
[7] C.Q. Li, M. Mahmoodian, Risk Based Service Life Prediction of Underground Cast Iron Pipes Subjected to Corrosion, vol. 119, Reliability Engineering & System Safety, 2013, pp. 102–108.
[8] B.B. Rajani, J.M. Makar, S.E. McDonald, Mechanical properties of grey cast iron water mains, ASCE, Journal of materials in Civil Engineering (2001) 1–45.
[9] J.F. Kiefner, P.H. Vieth, *A Modified Criterion for Evaluating the Remaining Strength of Corroded Pipe* (No. PR-3-805), Battelle Columbus Div., , OH (USA), 1989.
[10] M. Ahammed, R.E. Melchers, Reliability of underground pipelines subject to corrosion, J. Transport. Eng. 120 (6) (1994) 989–1002.
[11] H.P. Hong, Reliability based optimal inspection schedule for corroded pipelines, in: Proc. Annual Conference of the Canadian Society for Civil Engineering, 1998, pp. 743–752.
[12] B. Rajani, Y. Kleiner, Comprehensive review of structural deterioration of water mains: physically based models, Urban Water 3 (3) (2001) 151–164.
[13] B. Zhang, W. Wang, Y. Li, H. Lei, C.Q. Li, A Primary Relationship between Critical Strain Energy Density and Fracture Toughness of Mild Steel, Theoretical and Applied Fracture Mechanics, 2023, 104048.
[14] N.A. Barton, T.S. Farewell, S.H. Hallett, T.F. Acland, Improving pipe failure predictions: factors affecting pipe failure in drinking water networks, Water Res. 164 (2019), 114926.
[15] B.A. Wols, A. Vogelaar, A. Moerman, B. Raterman, Effects of weather conditions on drinking water distribution pipe failures in The Netherlands, Water Supply 19 (2) (2019) 404–416.
[16] S. Alvisi, M. Franchini, Comparative analysis of two probabilistic pipe breakage models applied to a real water distribution system, Civ. Eng. Environ. Syst. 27 (1) (2010) 1–22.
[17] C.Q. Li, Life cycle modelling of corrosion affected concrete structures – initiation, ASCE Journal of Materials in Civil Engineering 15 (6) (2003) 594–601.
[18] L. Scholten, A. Scheidegger, P. Reichert, M. Maurer, Combining Expert Knowledge and Local Data for Improved Service Life Modeling of Water Supply Networks, vol. 42, Environmental modelling & software, 2013, pp. 1–16.
[19] V. Kucera, E. Mattsson, Atmospheric corrosion, in: Corrosion Mechanisms, CRC Press, 2020, pp. 211–284.
[20] S. Hasan, F. Khan, S. Kenny, Probability assessment of burst limit state due to internal corrosion, Int. J. Pres. Ves. Pip. 89 (2012) 48–58.
[21] A.P. Teixeira, C.G. Soares, T.A. Netto, S.F. Estefen, Reliability of pipelines with corrosion defects, Int. J. Pres. Ves. Pip. 85 (4) (2008) 228–237.
[22] W.G. Wang, A. Zhou, G.Y. Fu, C.Q. Li, D. Robert, M. Mahmoodian, Evaluation of stress intensity factor for cast iron pipes with sharp corrosion pits, Eng. Fail. Anal. 81 (2017) 254–269.
[23] W. Wang, W. Yang, C.Q. Li, Fully plastic j-integrals for mixed mode fracture induced by inclined surface cracks in pressurized ductile pipes, Eng. Fail. Anal. 129 (2021), 105729.
[24] C.Q. Li, W. Yang, Time-dependent Reliability Theory and its Applications, Elsevier Science & Technology, 2022.
[25] R. Rackwitz, Reliability analysis—a review and some perspectives, Struct. Saf. 23 (4) (2001) 365–395.
[26] B.H. Zhang, Time-dependent reliability method and its application in mild steel pipelines, in: A Thesis Submitted in Fulfilment of the Requirements for the Degree of Doctor of Philosophy, 2023.
[27] Ø. Hagen, L. Tvedt, Vector process out-crossing as parallel system sensitivity measure, J. Eng. Mech. 117 (10) (1991) 2201–2220.
[28] O. Ditlevsen, H.O. Madsen, Structural Reliability Methods, vol. 178, Wiley, New York, 1996.
[29] D. Zwillinger, CRC Standard Mathematical Tables and Formulas, chapman and hall/CRC, 2018.
[30] B. Zhang, W. Wang, Y. Wang, X. Hu, C.Q. Li, An Improved Analytical Solution to Outcrossing Rate for Nonstationary and No-Gaussian Processes, Journal of Reliability Engineering & System Safety, 2023. A research paper submitted to the.
[31] J.R. Rice, A Path Independent Integral and the Approximate Analysis of Strain Concentration by Notches and Cracks, 1968.
[32] R.O. Ritchie, Mechanisms of fatigue-crack propagation in ductile and brittle solids, Int. J. Fract. 100 (1999) 55–83.
[33] B.E. Amstutz, M.A. Sutton, D.S. Dawicke, J.C. Newman, An Experimental Study of CTOD for Mode I/mode II Stable Crack Growth in Thin 2024-T3 Aluminum Specimens, vol. 1256, ASTM special technical publication, 1995, pp. 256–271.
[34] T.L. Anderson, Fracture Mechanics: Fundamentals and Applications, CRC press, 2017.
[35] M.G. Dawes, Elastic-plastic Fracture Toughness Based on the COD and J-Contour Integral Concepts, ASTM International, 1979, pp. 307–333.
[36] J.R. Rice, G. Rosengren, Plane strain deformation near a crack tip in a power-law hardening material, J. Mech. Phys. Solid. 16 (1) (1968) 1–12.
[37] C.F. Shih, Relationships between the J-integral and the crack opening displacement for stationary and extending cracks, J. Mech. Phys. Solid. 29 (4) (1981) 305–326.
[38] ASTM International, ASTM E1820-21: Standard Test Method for Measurement of Fracture Toughness, ASTM International, West Conshohocken, PA, 2021.
[39] J.D.G. Sumpter, C.E. Turner, Method for laboratory determination of je jc, Aug. 1975, in: Cracks and Fracture: Proceedings of the Ninth National Symposium on Fracture Mechanics: a Symposium Sponsored by Committee E-24 on Fracture Testing of Metals, vol. 601American Society for Testing and Materials, University of Pittsburgh, Pittsburgh, Pa, 1976, pp. 25–27, 2). ASTM International.
[40] X.K. Zhu, J.A. Joyce, Review of fracture toughness (G, K, J, CTOD, CTOA) testing and standardization, Eng. Fract. Mech. 85 (2012) 1–46.
[41] W. Wang, W. Yang, W. Shi, C.Q. Li, Modeling of corrosion pit growth for buried pipeline considering spatial and temporal variability, J. Eng. Mech. 147 (10) (2021), 04021065.
[42] I.S. Raju, J.C. Newman Jr., Stress-intensity factors for internal and external surface cracks in cylindrical vessels, J. Pressure Vessel Techol. 104 (4) (1982) 293–298.
[43] V.G.M.D. Kumar, M.D. German, C.F. Shih, *Engineering approach for Elastic-Plastic Fracture Analysis* (No. EPRI-NP–1931), General Electric Co, 1981.
[44] J.F. Knott, Fundamentals of Fracture Mechanics, Gruppo Italiano Frattura, 1973.
[45] M. Kutyłowska, M. Orłowska-Szostak, Comparative analysis of water–pipe network deterioration–case study, Water Pract. Technol. 11 (1) (2016) 148–156.
[46] H. Rezaei, B. Ryan, I. Stoianov, Pipe failure analysis and impact of dynamic hydraulic conditions in water supply networks, Procedia Eng. 119 (2015) 253–262.
[47] G. Fu, W. Yang, W. Deng, C.Q. Li, S. Setunge, Prediction of fracture failure of steel pipes with sharp corrosion pits using time-dependent reliability method with lognormal process, J. Pressure Vessel Technol. 141 (3) (2019).
[48] J. Ji, J.H. Lai, G. Fu, C. Zhang, J. Kodikara, Probabilistic failure investigation of small diameter cast iron pipelines for water distribution, Eng. Fail. Anal. 108 (2020), 104239.
[49] P. Rajeev, J. Kodikara, D. Robert, P. Zeman, B. Rajani, Factors contributing to large diameter water pipe failure, Water asset management international 10 (3) (2014) 9–14.
[50] W. Wang, Y. Wang, B. Zhang, W. Shi, C.Q. Li, Failure prediction of buried pipe network with multiple failure modes and spatial randomness of corrosion, Int. J. Pres. Ves. Pip. 191 (2021), 104367.